Time Series of Total Heating and Moistening over the Gulf of Carpentaria Radiosonde Array during AMEX

JOHN L. MCBRIDE, B. W. GUNN, G. J. HOLLAND, T. D. KEENAN AND N. E. DAVIDSON

Bureau of Meteorology Research Centre, Melbourne, Australia

WILLIAM M. FRANK

Department of Meteorology, The Pennsylvania State University, University Park, Pennsylvania

(Manuscript received 2 December 1988, in final form 13 June 1989)

ABSTRACT

Line integral techniques are used to calculate vertically integrated heat and moisture budgets over the Gulf of Carpentaria during Phase II of the Australian Monsoon Experiment (AMEX). The budget area is an array of six radiosondes in a monsoon environment, and the calculations are performed every 6 hours over a period of 33 days.

During convective outbreaks the integrated heating and drying of the large scale by the cumulonimbus activity has a magnitude of the order of 10°C day^{-1}. The heat and moisture sources are dominated by the flux divergence terms, which account for over 90% of the variance. The observed warming is as large as ±1°C day^{-1} but is diurnally dominated and does not correspond to the latent heat release. The integrated moisture convergence has a high correlation with latent heat release but not with the measured moisture storage. The convective heat source is also highly correlated with middle tropospheric vertical velocity.

Mean budgets are presented for each of the four diurnal observation times. Also, budgets were run with each station, in turn, excluded from the sonde array to determine sensitivity of the results to the data network.

1. Introduction

Dynamical studies of tropical weather are largely characterized by the specification of the heat and moisture source terms associated with cumulonimbus convection. One class of studies specifies the heating and studies the response of the system of equations (e.g., Gill 1980; Silva Dias et al. 1983; Hack and Schubert 1986). Another type of study specifies the heating in a simple functional form and analyzes the stability and structure of solutions to the resultant equation set (e.g., Charney and Eliassen 1964; Syono and Yamasaki 1966; Lau and Peng 1987). Even the numerical simulation of actual weather systems in the tropics tends to be preoccupied with the specification of the convective heat source at the initial time step (e.g., Puri 1985).

Despite the importance of the specification of these source terms, very few datasets exist that are suitable for their measurement under conditions of deep convective activity in the tropics. This study uses radiosonde data from the Australian Monsoon Experiment (AMEX) to analyze the dry static energy and moisture budgets of the Gulf of Carpentaria for individual time periods. This is equivalent to producing a time series of the total (or vertically integrated) sources of heat and moisture over the Gulf throughout the month-long experiment.

The background large scale flow conditions were those of a period of active monsoon, as will be documented in an accompanying paper by Gunn et al. (1989). Other aspects of the flow during the experiment plus preliminary research results on a variety of topics are described by McBride and Holland (1989).

Section 2 of the paper develops the mathematical framework for the analysis. The data and computational technique are described in the following two sections. Section 5 presents the results of the heat and moisture budgets. Section 6 contains an analysis of linear correlations between budget quantities and flow parameters. Section 7 presents mean budgets averaged over the time series, and section 8 contains sensitivity studies to the omission of stations from the radiosonde network. The results of the paper are summarized in the final section. There is no previous time series dataset of convective sources in a monsoon environment; so it is expected that the calculations presented here will be useful in many follow-up studies on cumulus parameterization theory and on the structure of individual weather systems.

Corresponding author address: Dr. John McBride, Bureau of Meteorology Research Centre, GPO Box 1289K, Melbourne 3001, Australia.

© 1989 American Meteorological Society

Unauthenticated | Downloaded 06/20/24 09:23 PM UTC

2. Equations and definitions

The thermodynamic equation and the moisture conservation equation can be written in the following form:

$$\frac{\partial s}{\partial t} + \nabla \cdot s\mathbf{v} + \frac{\partial \omega s}{\partial p} = L(c - e) + Q_R - \frac{\partial \omega' s'}{\partial p} \quad (1)$$

$$\frac{\partial q}{\partial t} + \nabla \cdot q\mathbf{v} + \frac{\partial \omega q}{\partial p} = (e - c) - \frac{\partial \omega' q'}{\partial p}. \quad (2)$$

In these equations, s is dry static energy ($=c_P T + gz$), q is mixing ratio of water vapor, ω is vertical (p-coordinate) velocity, L is the coefficient of latent heat, c and e are rates of condensation and evaporation, and Q_R is radiational heating. The terms with primes represent transports effected by subgrid scale eddies (including both turbulent fluxes at the surface and cumulonimbus up- and downdrafts).

If it is assumed the vertical motion is zero at 100 mb and at the surface, a vertical integration (with respect to p/g) yields the following forms of the above equations:

$$\left(\frac{\partial s}{\partial t}\right)^* + (\nabla \cdot s\mathbf{v})^* = LR_0 + S_0 + Q_R^* \quad (1a)$$

$$\left(\frac{\partial q}{\partial t}\right)^* + (\nabla \cdot q\mathbf{v})^* = -R_0 + E_0 \quad (2a)$$

where the superscript * denotes a term integrated from 100 mb to the surface, R_0 is precipitation at the surface, and S_0, E_0 are surface eddy fluxes of sensible heat and water vapor. By eliminating rainfall the equations can be combined:

$$\left(\frac{\partial s}{\partial t}\right)^* + (\nabla \cdot s\mathbf{v})^* + L\left(\frac{\partial q}{\partial t}\right)^* + L(\nabla \cdot q\mathbf{v})^* + \text{Resid} = 0 \quad (3)$$

where

$$\text{Resid} = -(Q_R^* + S_0 + LE_0). \quad (4)$$

In this paper, the first four terms of (3) will be calculated at each AMEX observation time. The sum of the first two terms equals the vertically integrated diabatic source term in the thermodynamic equation, i.e., the right-hand side of (1a). Similarly the next two terms equal the integrated source term in the moisture equation. Thus, defining the vertically integrated heat source as "Total Heating" and the vertically integrated moisture source as "Total Moistening," they can be expressed as follows:

$$\text{Total Heating} = \left(\frac{\partial s}{\partial t}\right)^* + (\nabla \cdot s\mathbf{v})^* \quad (5)$$

$$\text{Total Moistening} = \left(\frac{\partial q}{\partial t}\right)^* + (\nabla \cdot q\mathbf{v})^*. \quad (6)$$

3. Data

Radiosonde data were used from the array of stations surrounding the Gulf of Carpentaria (Fig. 1). The sondes were launched at 6 hour intervals with a success rate of 98%. The success rate for scheduled launches reaching the 100 mb level was 96%. The data used in this study were extracted from the real-time messages. The observers on station were instructed to insert 17 fixed levels into the significant level part of the WMO code. Combined with the mandatory levels these yielded a vertical resolution for wind data of better than 40 mb.

The period of study is from 1700 UTC 13 January to 2300 UTC 14 February 1987. This is slightly shorter than the period of AMEX, but is the period for which all six gulf stations were in operation.

The data were subjected to gross error and vertical and temporal consistency checks and were then linearly interpolated onto a 10 mb resolution vertical grid. The interpolation procedure included the hydrostatic recalculation of all heights. Missing data were then recovered by time interpolation of data from the same station, with a limit of two consecutive missing values. In 12 cases missing winds at 100 mb were replaced by the value at 150 mb. In three instances the 200 mb winds were extended upwards. This procedure yielded a complete set of data from the surface to 100 mb for the six stations, with the exception of two consecutive observation times on 9 February.

4. Line integral techniques

Trapezoidal line integrals were calculated along the boundaries of the array at the surface and every 50 mb from 100 to 950 mb. Application of Green's theorem in the plane (from classical vector analysis) yields the following quantities averaged over the area of the array:

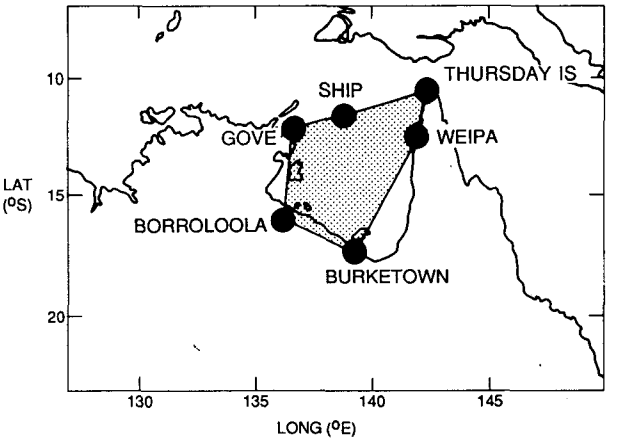

FIG. 1. The network of 6-hourly radiosonde stations surrounding the Gulf of Carpentaria during AMEX Phase II, 1987.

Unauthenticated | Downloaded 06/20/24 09:23 PM UTC

$$\text{Area} = \frac{1}{2}\oint (xdy - ydx) \tag{7}$$

$$\nabla \cdot \mathbf{v} = \frac{1}{(\text{Area})}\oint (udy - vdx) \tag{8}$$

$$\nabla \cdot (s\mathbf{v}) = \frac{1}{(\text{Area})}\oint (sudy - svdx) \tag{9}$$

$$\nabla \cdot (q\mathbf{v}) = \frac{1}{(\text{Area})}\oint (qudy - qvdx) \tag{10}$$

$$\text{Vorticity} = \frac{1}{(\text{Area})}\oint (udx + vdy). \tag{11}$$

The (x, y) position of each sonde at each vertical level was calculated from the reported winds and an assumed ascent rate. Vertical integrals of the above quantities were subsequently calculated trapezoidally. The vertical integral of divergence yielded a kinematic value of array-averaged vertical motion at each level. A constant mass-balance correction (MBC) was added to each divergence to ensure ω was zero at the surface and 100 mb. For consistency, this requires the calculation of a mass-balance correction for the budget quantities $\nabla \cdot s\mathbf{v}$, $\nabla \cdot q\mathbf{v}$. This is done by decomposing each horizontal flux divergence into a mean transport plus an eddy transport due to horizontal asymmetries:

$$\nabla \cdot s\mathbf{v} = \bar{s}(\nabla \cdot \mathbf{v}) + \text{Eddy} \tag{12}$$

where

$$\bar{s} = \left[\oint sdl\right]\left[\oint dl\right]^{-1} \tag{13}$$

and

$$dl = (dx^2 + dy^2)^{1/2}. \tag{14}$$

If $\nabla \cdot \mathbf{v}$ and $\nabla \cdot s\mathbf{v}$ are calculated from (8) and (9), then (12) is a definition of Eddy. Assuming the mass-balance correction to $\nabla \cdot s\mathbf{v}$ does not affect the horizontal eddy transport, then the mass-balanced flux divergence equals

$$(\nabla \cdot s\mathbf{v})_{\text{mass-balanced}} = \bar{s}(\nabla \cdot \mathbf{v} + \text{MBC}) + \text{Eddy}.$$
$$= \nabla \cdot s\mathbf{v} + \bar{s}\,\text{MBC}. \tag{15}$$

Henceforth all values of $\nabla \cdot \mathbf{v}$, $\nabla \cdot s\mathbf{v}$, $\nabla \cdot q\mathbf{v}$ described will be their mass-balanced values as calculated by the above procedure [with q transport calculated by the analogous relations to (12), (15)].

5. Budget results

a. Mass-balance correction

Figure 2 shows the time series of mass-balance correction. The units are mb day^{-1}, obtained by multiplying by the pressure depth of the troposphere (approximately 904 mb). The parallel lines on the plot correspond to the zero axis plus positive and negative corrections of 500 mb day^{-1}.

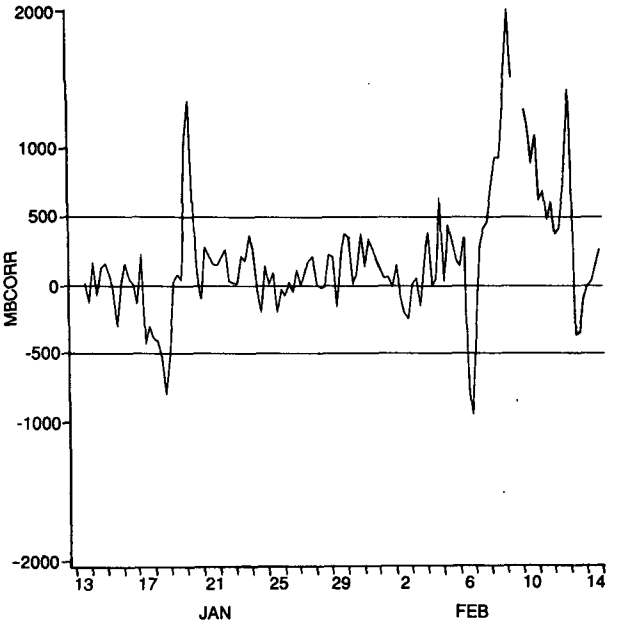

FIG. 2. Time series of mass-balance correction in mb day^{-1}. (A correction of 100 mb day^{-1} corresponds to a correction in divergence of 1.27×10^{-6} s^{-1}.)

The mass-balance correction can be interpreted as an inverse measure of the quality of the analysis of the divergent flow. Thus Fig. 2 reveals a short period in late January and a longer period towards the end of the experiment where the quality is poor, with corrections exceeding 600 mb day^{-1}. These correspond to times when tropical cyclones Irma and Jason were located within the Gulf of Carpentaria. Presumably the large corrections reflect an inability of the six sonde stations to resolve the cyclones' (smaller scale) circulation features. For the remaining 82% of the time series the analysis quality seems quite good with the mean of the absolute value of the correction equalling 178 mb day^{-1} (corresponding to a divergence of 2.3×10^{-6} s^{-1}) and a standard deviation of 141 mb day^{-1} (1.8×10^{-6} s^{-1}). Analysis times with corrections exceeding 600 mb day^{-1} in magnitude will be omitted from the analyses and time series in the remainder of the paper.

For comparison, Frank (1979) in his budget analysis of individual time periods during the GARP Atlantic Tropical Experiment (GATE) used a cutoff value of 4×10^{-6} s^{-1}. The GATE array is larger than AMEX (approximately 3.5 deg latitude compared with 2.7 deg latitude in radius); thus the same error assumed in the divergent component of wind in GATE would be equal to a mass-balance correction cutoff in AMEX of 5.2×10^{-6} s^{-1} or 400 mb day^{-1}.

Unauthenticated | Downloaded 06/20/24 09:23 PM UTC

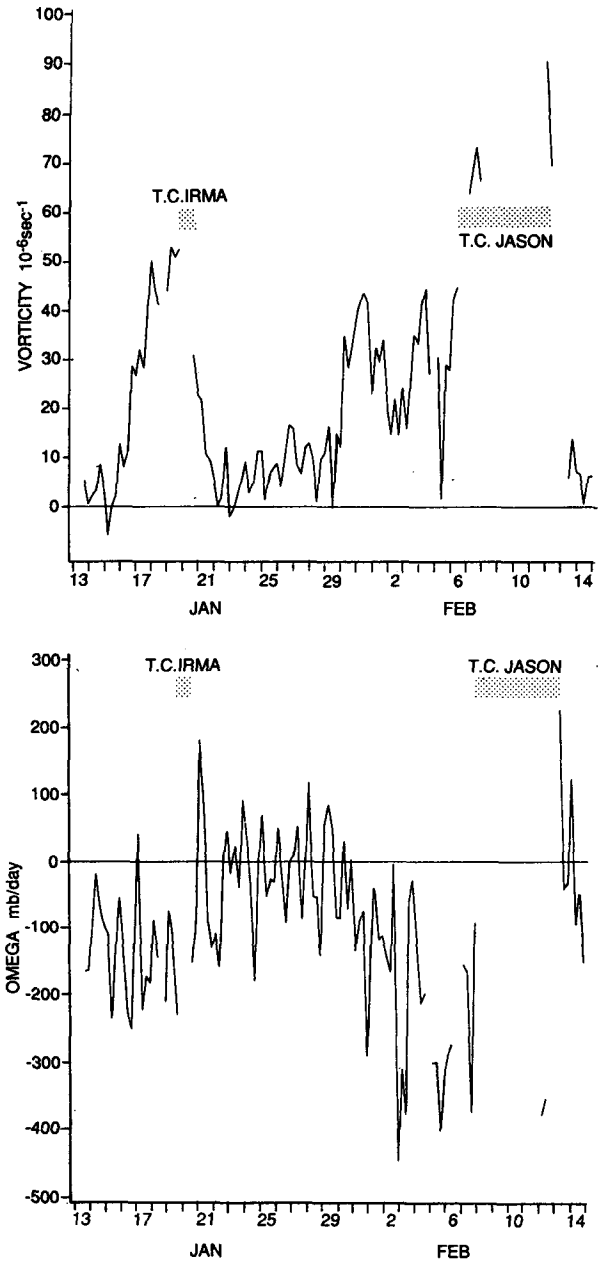

FIG. 3. Time series of relative vorticity (cyclonic positive) and vertical motion (upwards negative) at 700 mb. Also shown are the periods when tropical cyclones Irma and Jason were present within the sonde array. All quantities in this and following figures are calculated by line integral techniques over the array shown in Fig. 1. Times when the mass balance correction exceeds 600 mb day^{-1} have been omitted and appear as blanks on this and subsequent figures.

b. *Kinematic time series*

The kinematic nature of the flow over the array is characterized in Fig. 3 by the time series of vertical motion ω (negative upwards) and relative vorticity ζ (positive cyclonic) at 700 mb. The vertical motion field exhibits upward motion to about 21 January, followed by 8 days with ω fluctuating around zero, then large negative ω to the end of the experiment. The ζ field is cyclonic during the two upward (active monsoon) periods and close to zero during the inactive monsoon period. During the two active regimes, however, ζ tends to increase gradually from one day to the next, whereas ω fluctuates about a mean value.

Figure 3 also shows the durations of the two tropical cyclones within the sonde array. Note that both developed at times when the background relative vorticity (i.e., over the scale of the gulf) was quite large. Note also that most of the omitted data (blank spaces on the graph) correspond to when cyclone Jason was within the array.

c. *Heating and moistening*

Considering the measured components of vertically integrated diabatic heating and convective moistening, Fig. 4 shows time series of each of the first four terms of Eq. (3), all expressed in atmospheric heating rate units of °C day^{-1}. The $(\nabla \cdot v\bar{s})^*$ and $(\nabla \cdot v\bar{q})^*$ are seen to be of opposite phase, there being large magnitude integrated dry static energy divergence and moisture convergence during the periods of convective (or monsoon) activity. This corresponds to cumulonimbus activity acting as a *heat source* and a *moisture sink* to the larger scale flow, as documented and discussed by Gray (1973), Yanai et al. (1973), Betts (1978) and others.

During the convective outbreaks the magnitudes of $(\nabla \cdot v\bar{s})^*$ and $(\nabla \cdot v\bar{q})^*$ are of the order of 10°C day^{-1}. The tendencies, $(\partial \bar{s}/\partial t)^*$, $(\partial \bar{q}/\partial t)^*$, are usually an order of magnitude smaller; hence from (5) and (6) the Total Heating and Total Moistening are of the order of + and −10°C day^{-1} respectively.

As a check that the simultaneous occurrences of large magnitude, opposite phase values of $(\nabla \cdot v\bar{s})^*$ and $(\nabla \cdot v\bar{q})^*$ do actually correspond to outbreaks of convection, a time series was constructed of one other approximate measure of convective activity—Percentage High Cloud (PHC). PHC is defined as the mean over the area of the gulf of geostationary satellite black body temperature pixels less than −55°C. The linear correlation coefficient between the time series of PHC and $(\nabla \cdot v\bar{s})^*$ is 0.68 and that between PHC and $(\nabla \cdot v\bar{q})^*$ is −0.61. Since PHC is itself only an approximate measure of convective activity, these correlations are considered to be large enough to justify our interpretation of the $(\nabla \cdot v\bar{s})^*$, $(\nabla \cdot v\bar{q})^*$ time series.

Inspection of Fig. 4b reveals that $(\partial \bar{s}/\partial t)^*$ is dominated by a diurnal oscillation which corresponds to a variation in $\bar{s}^*$ of amplitude approximately 0.52°C from peak to trough. This occurs over 12 hours corresponding to a warming rate of 1.04°C day^{-1}. It is not a result of boundary layer heating along the coastline on which the sondes are located as it appears (with some variation in phase) throughout the entire depth

Unauthenticated | Downloaded 06/20/24 09:23 PM UTC

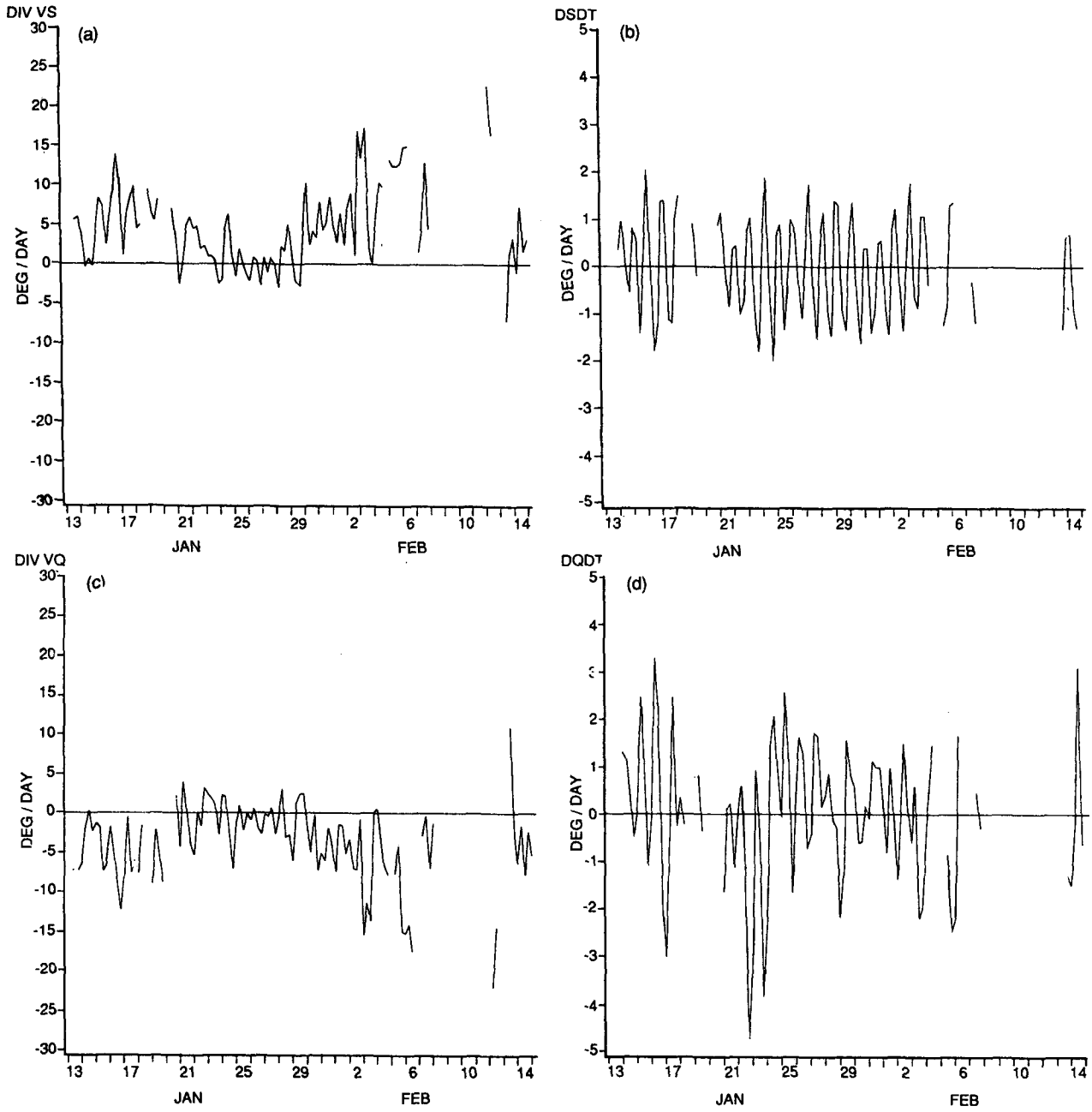

FIG. 4. Time series of budget quantities vertically integrated from 100 mb to the surface and converted to mean tropospheric heating rate units of °C day^{-1}. (a) $\nabla \cdot sv$, (b) $\partial s/\partial t$, (c) $\nabla \cdot qv$, (d) $\partial q/\partial t$.

of the troposphere. From comparison with the studies of Foltz and Gray (1979) and Frank (1980) on the diurnal variation of tropospheric temperatures, this oscillation is presumably real and is related to the diurnal tides. (It should be noted that standard radiation error corrections have been applied to all sonde measurements with the exception of those at Gove.)

The interest in the current study is in fluctuations in $(\partial s/\partial t)^*$ associated with fluctuations in convective activity. Accordingly the convective/synoptic signal was obtained by subtracting the experiment-mean value of the diurnal variation from each observation of $(\partial s/\partial t)^*$. The resulting time series (Fig. 5) shows irregular fluctuations of less than 1°C day^{-1} in amplitude and bearing no relationship to the convective outbreaks reflected in the time series of $(\nabla \cdot sv)^*$ and $(\nabla \cdot qv)^*$. In Fig. 4d, a diurnal variation is also apparent in $(\partial q/\partial t)^*$; but subtraction of the mean value for each

Unauthenticated | Downloaded 06/20/24 09:23 PM UTC

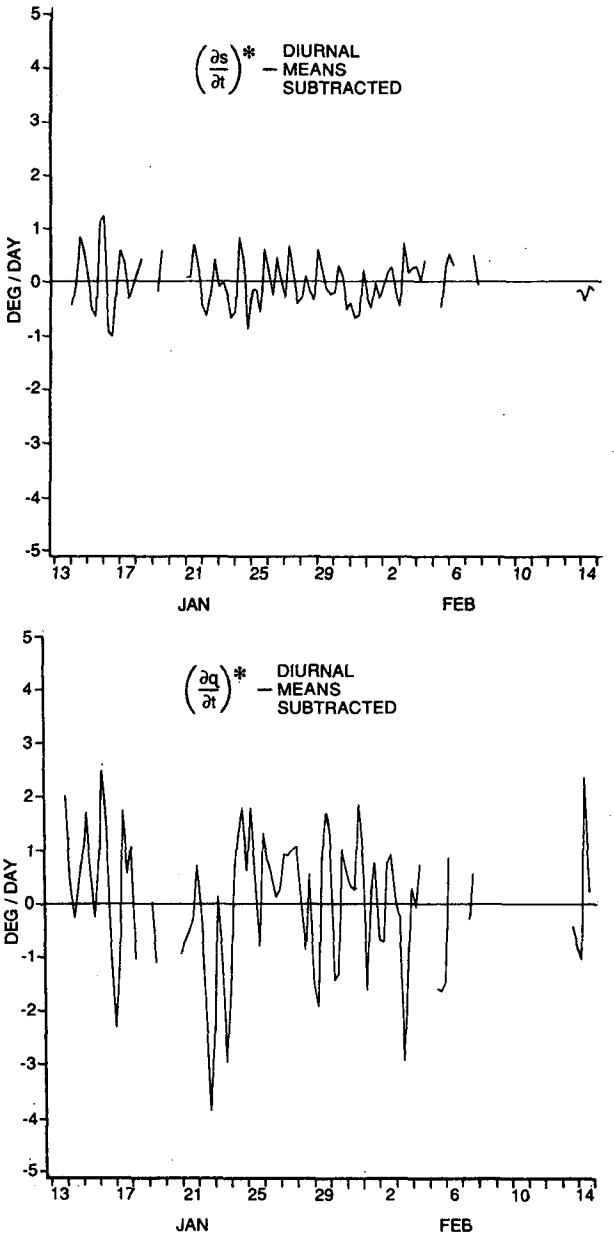

FIG. 5. Time series of vertically integrated $\partial s/\partial t$, $\partial q/\partial t$ after the experiment-mean diurnal variation of each quantity has been removed.

observation time (Fig. 5) does not fundamentally change the character of the time series. Quantitatively, subtraction of the experiment-mean diurnal variation reduces the variance of the $(\partial q/\partial t)^*$ time series by only 25%, whereas for the $(\partial s/\partial t)^*$ series the reduction is 81%. Thus it must be concluded that the $(\partial q/\partial t)^*$ variations are associated with synoptic and convective phenomena. It is also noteworthy that on occasion $(\partial q/\partial t)^*$ is comparable in magnitude to $(\nabla \cdot s\mathbf{v})^*$ and $(\nabla \cdot q\mathbf{v})^*$. Thus the moisture tendency can be a significant term in Eq. (3), a result of some importance for the theory of cumulus parameterization.

Referring back to the time series of $(\nabla \cdot s\mathbf{v})^*$, $(\nabla \cdot q\mathbf{v})^*$ in Fig. 4, these variables also reflect the quiet/suppressed period separating two convectively enhanced periods already discussed in association with Fig. 3. The peaks in convective activity have a one-to-one association in the two series. They also have a pronounced phase locking as shown in Fig. 6. The peaks occur most frequently with data from sondes launched at 1600 and 2200 UTC (corresponding to 0200 and 0800 Local Time). This agrees with satellite observations of convective activity over the gulf, as will be documented in a separate study.

As noted above, during the convective outbreaks $(\nabla \cdot s\mathbf{v})^*$ and $L(\nabla \cdot q\mathbf{v})^*$ are in approximate balance. Their sum, $(\nabla \cdot h\mathbf{v})^*$, is a measure of whether the divergent circulation of the weather system imports or exports total energy. The time series of $(\nabla \cdot h\mathbf{v})^*$ is shown in Fig. 7. It is seen that during the periods of convective activity at the start and end of the experiment, the divergent circulation exported energy, the source being surface fluxes of latent and sensible heat [through Eq (3)]. Conversely during the suppressed period, $(\nabla \cdot h\mathbf{v})^*$ was negative, meaning that radiative energy loss exceeded the surface input.

6. Correlations

As discussed in the Introduction, a primary component of tropical dynamics is the specification of Total

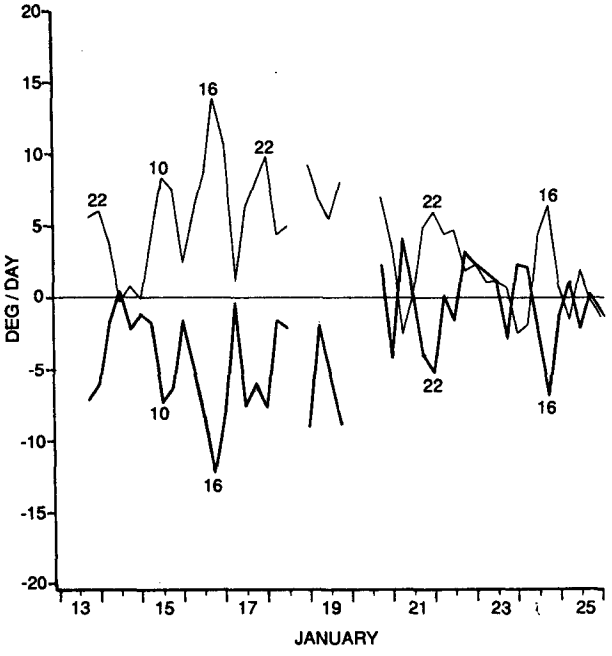

FIG. 6. Close-up of a section of Figs. 4a and 4c overlaid onto one graph. The light curve is $\nabla \cdot s\mathbf{v}$. The heavy curve is $\nabla \cdot q\mathbf{v}$. The numbers on selected peaks and troughs represent the UTC time of that observation.

Unauthenticated | Downloaded 06/20/24 09:23 PM UTC

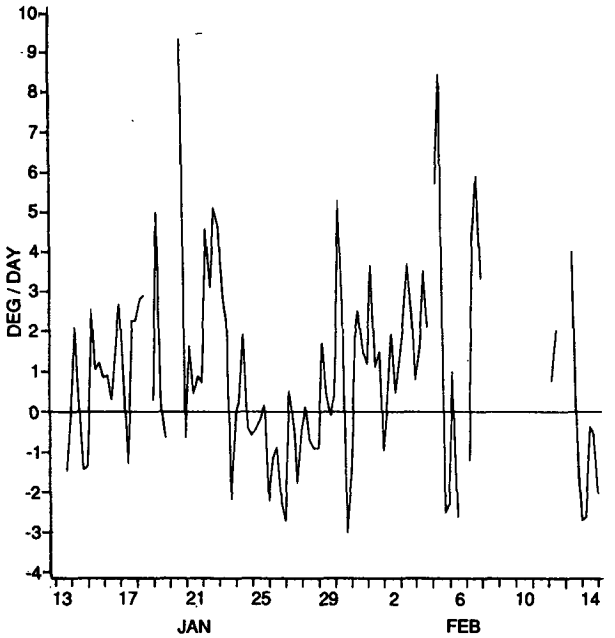

FIG. 7. Time series of vertically integrated $\nabla \cdot hv$.

Heating and Total Moistening in terms of the other dependent variables in the equation set. This is a component of the *cumulus parameterization* problem. The constraint expressed through (3), (4) and (6) means this is equivalent to expressing any of the terms of (3) as functions of other dependent variables. To provide insight into this problem, all time series analyzed for the sonde array have been linearly correlated.

Table 1 shows the resultant correlation coefficients between Total Heating (TH), Total Moistening (TM) and each of the measured terms of Eq. (3). Total Heating correlates with $(\nabla \cdot sv)^*$ at a value of 0.98, confirming the conclusion implied throughout the previous section that on this 6-hourly measurement time scale these two variables are essentially interchangeable. Similarly variations in TM are dominated by those of $(\nabla \cdot qv)^*$, which at a correlation of 0.95 account for 90% of the variance.

The correlations of the four terms of (3) with each other are shown in Table 2. The only large value seen is the correlation between $(\nabla \cdot sv)^*$ and $L(\nabla \cdot qv)^*$, which has a value of −0.9, accounting for over 80% of the variance. On the other hand, the tendency terms $(\partial s/\partial t)^*$, $(\partial q/\partial t)^*$ have effectively zero correlation with each other and with the integrated flux divergence terms. These correlations have a number of interesting implications.

TABLE 2. Matrix of linear correlation coefficients over the time series for the terms of Eq. (3). The first entry is for $(\partial s/\partial t)^*$ after subtracting the experiment–mean value for that observation time [i.e., Diurnal Mean Subtracted (DMS)].

	$(\partial s/\partial t)^*$DMS	$(\partial s/\partial t)^*$	$(\nabla \cdot sv)^*$	$(\partial q/\partial t)^*$	$(\nabla \cdot qv)^*$
$(\partial s/\partial t)^*$DMS	1	—	−0.01	—	0.04
$(\partial s/\partial t)^*$		1	−0.06	0.02	0.09
$(\nabla \cdot sv)^*$			1	−0.08	−0.90
$(\partial q/\partial t)^*$				1	0.06

First, they substantiate our interpretation of Figs. 4 and 6 that the convective outbreaks are characterized by simultaneous peaks in $(\nabla \cdot sv)^*$ and $L(\nabla \cdot qv)^*$ of opposite phase. The very large correlation between these two variables also substantiates the vertical constraint philosophy of Kuo-type convective parameterization schemes (Kuo 1974; Anthes 1977; Krishnamurti et al. 1976) that variations in latent heat release $(\nabla \cdot sv)^*$ are determined by variations in integrated moisture convergence $-(\nabla \cdot qv)^*$.

Second, there is effectively zero correlation between the realized warming $(\partial s/\partial t)^*$ and either of $(\nabla \cdot sv)^*$ (Table 2) or Total Heating (Table 1). This same finding was made by Frank (1980) in GATE. Following Frank's reasoning, it means that latent heat release did not produce significant changes in the net tropospheric sensible heat content on the observed time (6 hour) and space (500 km) scales. Since the rate of condensation heating of the gulf often exceeded 10°C day^{-1} (Figs. 4 and 6), clearly the energy was dispersed rapidly to larger scales.

Third, the above-mentioned Kuo-type parameterizations also use a relationship (referred to as the *b*-parameter) between the moisture tendency and integrated moisture convergence. The zero correlation between $(\partial q/\partial t)^*$ and $(\nabla \cdot qv)^*$ in Table 2, however, shows that over the gulf during AMEX, no such relationship existed.

Table 3 shows coefficients of correlation between the terms of Eq. (3) and various other large scale parameters, while (for completeness) Table 4 shows the

TABLE 1. Linear correlation coefficients between Total Heating (TH), Total Moistening (TM) and each of the measured terms of Eq. (3).

	TH	TM
$(\partial s/\partial t)^*$	0.16	0.09
$(\nabla \cdot sv)^*$	0.98	−0.85
$(\partial q/\partial t)^*$	−0.07	0.37
$(\nabla \cdot qv)^*$	−0.86	0.95

TABLE 3. Linear correlation coefficients between the terms of Eq. (3) and other large scale parameters.

	$\bar{s}$	$\bar{q}$	ζ_{700}	ω_{700}	Julian day
$(\partial s/\partial t)^*$DMS	−0.00	−0.03	0.12	0.07	0.02
$(\partial s/\partial t)^*$	0.02	−0.14	0.01	0.15	−0.02
$(\nabla \cdot sv)^*$	−0.27	0.31	0.54	−0.91	0.38
$(\partial q/\partial t)^*$	0.22	−0.01	−0.07	0.06	−0.12
$(\nabla \cdot qv)^*$	0.38	−0.21	−0.46	0.87	−0.36

Unauthenticated | Downloaded 06/20/24 09:23 PM UTC

TABLE 4. Remaining linear correlation coefficients necessary to complete a correlation matrix when added to Tables 1 to 3.

	TH	TM	$\bar{s}$	$\bar{q}$	ζ_{700}	ω_{700}	Julian day
TH	1	−0.82	−0.29	0.30	0.42	−0.86	0.35
TM		1	0.48	−0.25	−0.31	0.82	−0.37
$\bar{s}$			1	−0.15	−0.12	0.34	−0.41
$\bar{q}$				1	0.21	−0.26	−0.06
ζ_{700}					1	−0.48	0.37
ω_{700}						1	−0.37

remaining correlations possible between the variables in Tables 1–3. From Table 3, we see $(\nabla \cdot s\mathbf{v})^*$ and $(-\nabla \cdot q\mathbf{v})^*$ are significantly correlated with the day number, implying a linear trend of these variables through the time series. Both variables are also highly correlated with both ζ and ω at 700 mb. The correlation with ω is consistent with that found by Song and Frank (1983) between latent heat release and midtropospheric vertical velocity in GATE. The correlations between the convective sources and ζ are possibly not causal but could result from both being independently correlated with ω and/or day number. This also should be investigated further.

7. AMEX mean budgets

An assessment of the accuracy of the budgets can be obtained by considering how well they balance when averaged over the time series. Following Frank (1979) and Albright et al. (1981), the mean budgets can be expressed in terms of budget-diagnosed precipitation. There are two estimates available: from the s-budget [based on Eq. (1a)] and from the q-budget [Eq. (2a)].

The resultant experiment-mean estimates of the precipitation at each observation time are given in Tables 5 and 6. Values of mean tropospheric radiative heating are taken from the calculations of Cox and Griffith (1979) for conditions of enhanced convective activity in GATE (Cox and Griffith's Table 6). The values of surface evaporation and sensible heat flux are bulk aerodynamic estimates calculated at each observation time using the same formulae and drag coefficients as were used by Frank (1979) for GATE. For the bulk aerodynamic calculation, surface wind speed over the gulf was estimated by taking the perimeter average of the wind speed at 900 mb and multiplying by 0.8 to account for frictional retardation below that level; temperature and moisture were perimeter average surface values; and sea surface temperatures were based on observations from ships within the gulf.

TABLE 5. Experiment-mean dry static energy budget at each observation time.

	Heat budget (deg day^{-1})				
	$(\partial s/\partial t)^*$	$(\nabla \cdot s\mathbf{v})^*$	$-Q_R^*$	$-S_0$ =	LR_0
0400 UTC (1400 Local)	1.1	4.8	0.2	−0.01	6.1
1000 UTC (2000 Local)	−0.8	5.2	1.6	−0.2	5.8
1600 UTC (0200 Local)	−1.1	5.2	1.6	−0.3	5.4
2200 UTC (0800 Local)	0.8	4.3	1.0	−0.2	5.9

TABLE 6. Experiment-mean moisture budget at each observation time.

	Moisture budget (°C day^{-1})			
	$-(\partial q/\partial t)^*$	$-(\nabla \cdot q\mathbf{v})^*$	$+E_0$ =	R_0
0400 UTC (1400 Local)	−0.8	3.1	1.8	4.1
1000 UTC (2000 Local)	−0.7	3.7	2.0	5.0
1600 UTC (0200 Local)	0.8	4.6	1.9	7.3
2200 UTC (0800 Local)	0.7	4.3	1.6	6.6

The s-budget calculations in Table 5 yield an even distribution of precipitation throughout the diurnal cycle, whereas the moisture budget calculations (Table 6) give a precipitation maximum around 1600–2200 UTC. The latter calculation agrees with satellite imagery over the gulf. One possible source of error in the budgets is an inability to measure the true diurnal variation of temperature and moisture over the sonde array with soundings only on the perimeter. Accordingly, Table 7 shows experiment-mean budgets with the tendency terms $[(\partial s/\partial t)^*, (\partial q/\partial t)^*]$ omitted from the calculation. This procedure does produce a diurnal variation in s-budget diagnosed precipitation, but it is out of phase with that obtained from the moisture budget.

Another possible source of error arises from the use of the mass-balance correction cutoff of 600 mb day^{-1}. This means that individual time periods are omitted from the life cycles of weather systems. A possible remedy would be to average only those days for which all four times show mass-balance correction below the threshold. This will be a topic for further investigation.

Besides the differences in diurnal variation, the budget estimates in Tables 5 and 6 also differ in absolute magnitude. The difference between the estimates at each observation time is equal to the correction (or error) term required for balance of the moist static

TABLE 7. Budget estimates of precipitation (converted to units of °C day^{-1}) when the tendency terms are omitted from the calculations in Tables 5 and 6.

	s-budget	q-budget
0400 UTC (1400 Local)	5.0	4.9
1000 UTC (2000 Local)	6.6	5.7
1600 UTC (0200 Local)	6.5	6.5
2200 UTC (0800 Local)	5.1	5.9

Unauthenticated | Downloaded 06/20/24 09:23 PM UTC

energy budget [Eq. (3)]. These corrections are −2.0, −0.8, 1.9 and 0.7°C day^{-1} at 0400, 1000, 1600 and 2200 UTC respectively. These errors are of comparable magnitude to all other terms in the budget equations, and are too large to be significantly altered by errors in our estimates of radiation or surface fluxes.

It follows that the errors in the calculations of the heat and moisture sources at individual time periods are also of at least this magnitude. This seems large, although as Figs. 4 and 5 show, the magnitudes of the sources during convective outbreaks can be as large as 10–15°C day^{-1}. Thus, it should be expected that the time series of budget-diagnosed heating and drying presented in this paper are qualitatively correct, but that at any individual time period the actual magnitudes may be in error by as much as 2°C day^{-1}.

Throughout this paper reference has been made to similar budget calculations using data from GATE (e.g., Frank 1979, 1980; Albright et al. 1981). Accordingly, it is appropriate to compare the above error estimates with those in GATE. Albright et al. (1981) carried out for GATE the same calculations as shown in Tables 5 and 6. Their calculation procedure differed from the current paper in that they fitted quadratic surfaces to each variable in their sonde array at each level, rather than using line integrals. They also calculated the source terms in advective rather than flux form.

The required corrections for balance of the moist static energy budget in GATE at four observation times can be obtained by subtracting row 7 of Table 1 from row 6 of Table 3 of Albright et al. Converted to the units of this paper, the corrections are 0.8, 1.4, 0.7 and −0.1°C day^{-1} at 2230, 0430, 1030 and 1630 Local Time. These corrections are approximately half the values obtained above for the current AMEX study. A reasonable conclusion is that the errors at individual times follow the same ratio; that is, the errors in AMEX are approximately twice those in GATE. As has been discussed above, this difference is partly attributable to the larger size of the GATE array so that the same wind error in both experiments would yield a larger divergence error for AMEX compared with GATE. Another major difference between networks is the very even spacing of the sonde sites around the GATE A/B array compared with the very uneven spacing for AMEX (Fig. 1).

8. Sensitivity to number of stations in the network

The remoteness of northern Australia makes the establishment of a sonde network, such as that in Fig. 1, an expensive venture. The location and number of sondes were based on logistical and financial considerations, as well as meteorological ones. It is thus appropriate to consider the sensitivity of the results to the presence/absence of each individual station in the array.

As has been discussed, most of the information content of the budgets lies in the time series of $(\nabla \cdot sv)^*$ and $(\nabla \cdot qv)^*$. To gauge the importance of each station, these time series are shown in Figs. 8b–g, with each station omitted in turn from the line integral calculation. For comparison, the series for the calculation based on all six stations is shown on the same scale in Fig. 8a.

The most obvious feature seen in the comparison of the seven parts of the figure is that the data gaps are different. As with earlier figures, a time period is omitted whenever the mass-balance correction exceeds 600 mb day^{-1}. The proportion of the time series satisfying this criterion is shown in Table 8. Removal of Gove, Thursday Island or the Chinese (PRC) ship makes little difference to the quality of the budgets as measured by this criterion, whereas removal of any of the other three stations brings about a major degradation in quality. (Omission of Gove actually gives a slight increase in the proportion of the time series within the mass-balance cutoff. This is a spurious effect associated with time periods when a tropical cyclone is close to Gove and does not imply any improvement in analysis quality.)

One other feature of Fig. 8 is the close correspondence between the peaks and troughs of the time series for the different networks. This is demonstrated quantitatively in Table 9 for the three 5-station networks with similar mass-balance corrections to the total network.

The very high correlations shown between the 5-station calculations and the original time series show that the results of this paper are relatively insensitive to the exclusion of Gove, Thursday Island or the PRC ship from the sonde array. This result was unexpected. It raises the question of how many stations are needed to perform budget calculations. In particular, are the four northern stations in Fig. 1 sufficient to carry out budgets for the northern part of the array?

To address this, the time series of mass-balance corrections for the small array of Gove, Weipa, Thursday Island, and the PRC ship is shown in Fig. 9. Data gaps correspond to periods when the mass-balance correction is beyond the limits of the graph; i.e., its magnitude exceeds 2000 mb day.$^{-1}$ Comparison with Fig. 2 reveals that four stations are not enough to obtain reliable line integral values of divergence at individual time periods. The proportion of the series within the mass-balance correction cutoff of 600 mb day^{-1} is only 52% as compared with 82% for the complete network. It is likely, however, that this result is largely influenced by the odd shape of this particular four station array.

It is appropriate to emphasize that the 600 mb day^{-1} cutoff removed 23 time periods from the original (6-station) time series. For 19 of the 23 times, a fully developed tropical cyclone (Irma or Jason) was within the array. The results of the sensitivity analysis in this section, therefore, apply essentially to the nontropical

Unauthenticated | Downloaded 06/20/24 09:23 PM UTC

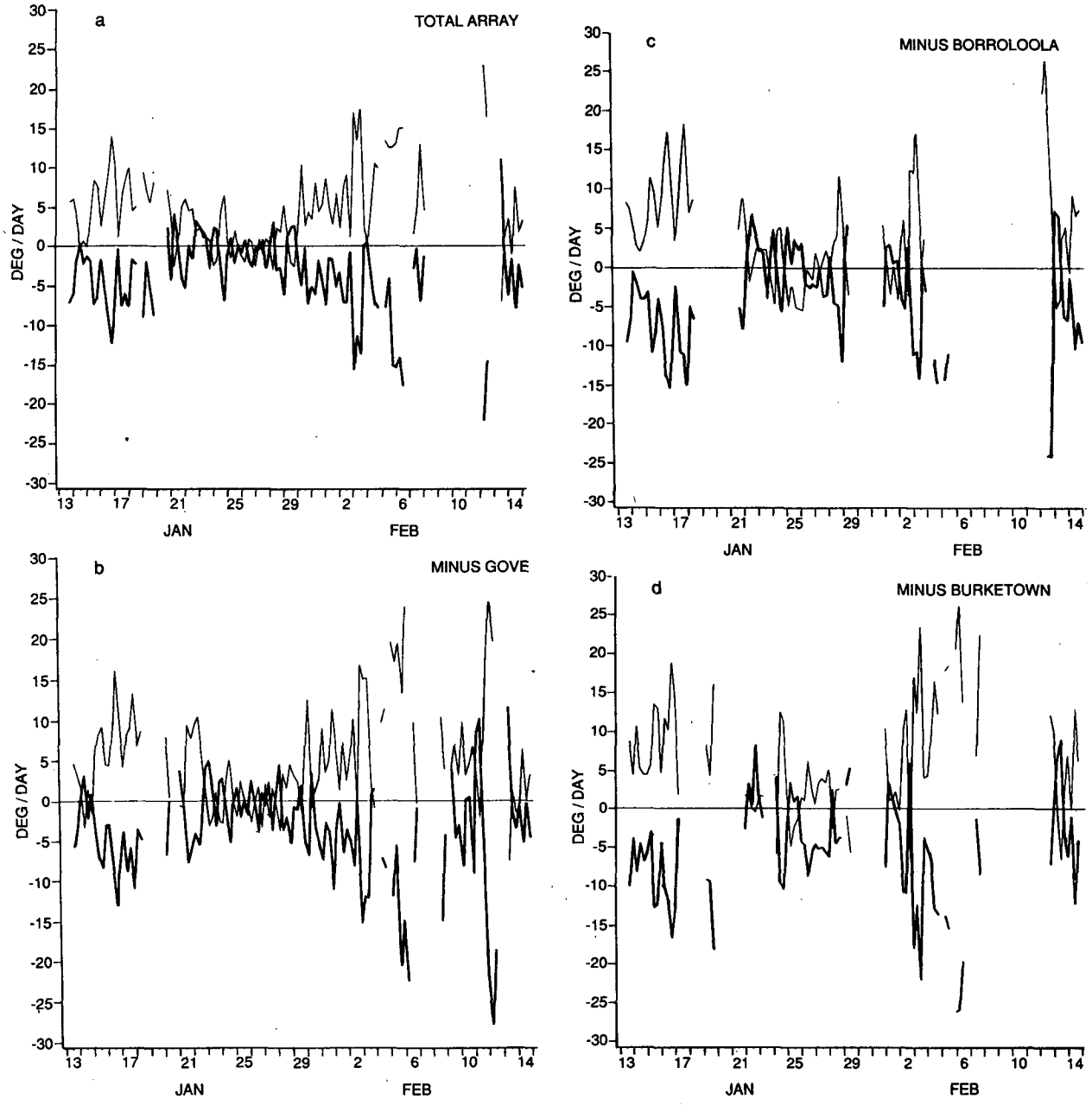

FIG. 8. Time series of $\nabla \cdot sv$ (light curve) and $\nabla \cdot qv$ (heavy curve). (a) For the network in Fig. 1, (b) for that network with Gove omitted from the line integral calculations, (c) for the network with Borroloola omitted, (d) with Burketown omitted,

cyclone periods during AMEX. For example, in Table 8 the life cycles of the cyclones are during the missing 18% of the 6-station entry. Thus the further degradation to 63% when Burketown is omitted is a degradation not associated with tropical cyclones.

9. Summary and conclusions

The above results provide information on two separate issues. The first is whether the placement of AMEX radiosondes around the Gulf of Carpentaria sufficiently provided time series measurements of convective heat and moisture sources. The second is what these measurements tell us about the relationships between the convective sources and the larger scale flow patterns.

Addressing the former issue, the only previous tropical dataset used to derive time series of the convective source terms is that from GATE (Frank 1979; Song and Frank 1983). The usual measure of quality of divergence calculations is the mass-balance correction (MBC). From Fig. 2, for AMEX the demarcation be-

Unauthenticated | Downloaded 06/20/24 09:23 PM UTC

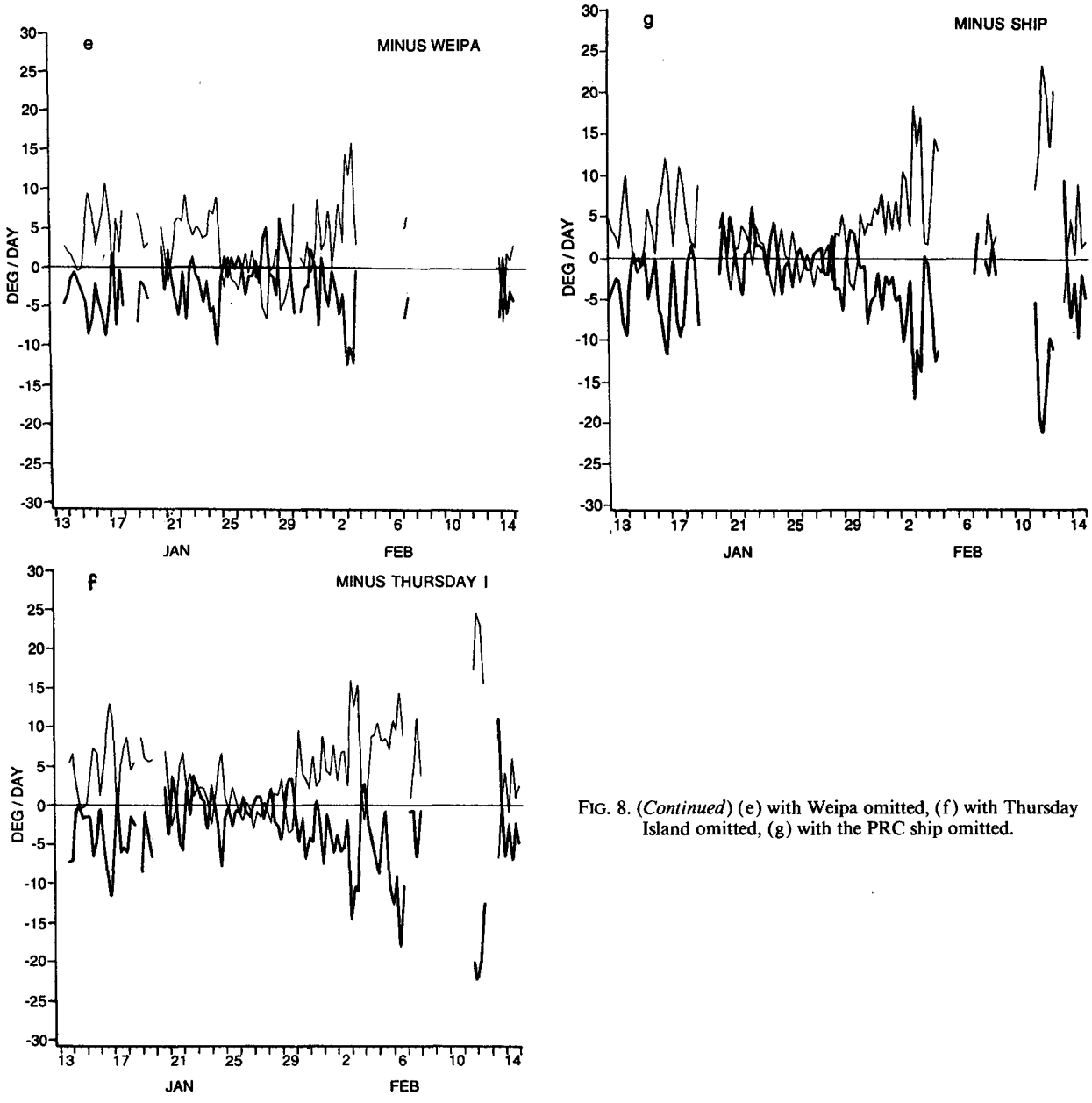

FIG. 8. (*Continued*) (e) with Weipa omitted, (f) with Thursday Island omitted, (g) with the PRC ship omitted.

tween a normal analysis time and one of large mass-balance correction corresponded to an MBC value of around 600 mb day^{-1}. This is approximately twice the value used as a cutoff for GATE data by Frank (1979). It is noted, however, that the GATE sonde array was approximately 60% larger than the Gulf of Carpentaria, so a given error in the normal component of wind yields a larger divergence error in AMEX than in GATE. Use of this cutoff retained essentially the whole AMEX time series *except for the periods when a tropical cyclone was present in the array.*

These large mass-balance corrections in the presence of tropical cyclones are a cause for concern. Understanding of the large scale budgets of heat, moisture and angular momentum is necessary for the understanding of development and maintenance of the tropical cyclone's circulation (for example, see Anthes 1974; Frank 1977; McBride 1981; Ooyama 1982). The implication of the large mass-balance corrections observed in AMEX, however, is that even when the cyclone is totally within a network of six radiosondes, the data resolution is insufficient to yield meaningful calculations of budget quantities at individual time periods.

Very large mass-balance corrections resulted also when attempts were made to perform budgets from

Unauthenticated | Downloaded 06/20/24 09:23 PM UTC

TABLE 8. Proportion of the time series for which the mass balance correction is less than 600 mb day^{-1}. Figures are given for all six stations and for the various combinations of five stations.

All six stations	82%
Excluding Gove	87%
Excluding Borroloola	66%
Excluding Burketown	63%
Excluding Weipa	66%
Excluding Thursday Island	84%
Excluding PRC ship	83%

the northern subarray of four stations. This would seem to indicate that any budgets of convective situations based purely on data from four or fewer radiosonde stations should be treated with suspicion.

Moving on to the actual findings of the AMEX budgets, the time series of budget quantities was dominated by variations in the integrated flux divergence terms, $(\nabla \cdot sv)^*$ and $(\nabla \cdot qv)^*$. During the diagnosed convective outbreaks these two fluxes showed large magnitudes of opposite sign, corresponding to a heating and drying of the large scale by the cumulonimbus activity. This simultaneous opposite-phase variation is observational support for the concept that latent heat release is linearly related to integrated moisture convergence. Variations in the latent heat release (and the moisture sink) were also closely related to variations in midtropospheric vertical motion and (to a lesser extent) relative vorticity.

The variations in observed warming $(\partial s/\partial t)^*$ were dominated by a diurnal oscillation and showed no correspondence with the diagnosed latent heat release, agreeing with the results of Frank (1980) for GATE. Variations in moisture tendency $(\partial q/\partial t)^*$ were occasionally of comparable magnitude to the horizontal flux terms, but showed no strong statistical relationship to variations in any other variable, including integrated moisture convergence.

Convective activity, as diagnosed from $(\nabla \cdot sv)^*$ and $(\nabla \cdot qv)^*$, also showed a diurnal modulation with peaks in the two source terms occurring most frequently at 1600 and 2200 UTC.

The export of moist static energy $(\nabla \cdot hv)^*$ was generally positive, reflecting the role played by tropical weather systems as sources of energy to the larger scale flow.

Mean budgets were presented for each observation time. These revealed an inconsistency between the heat and moisture budgets, but still should provide insight into the mean state of the tropical atmosphere during the experiment. Sensitivity studies reveal the time series budgets to be relatively insensitive to the omission of Gove, the ship or Thursday Island from the network. The budgets were greatly affected, however, by omission of any of the other three stations.

TABLE 9. Linear correlation coefficients between values of $(\nabla \cdot sv)^*$, $(\nabla \cdot qv)^*$ calculated from the specified five station networks and values from the complete network.

	$(\nabla \cdot sv)^*$	$(\nabla \cdot qv)^*$
Excluding Gove	0.93	0.91
Excluding Thursday Island	0.97	0.97
Excluding PRC ship	0.93	0.92

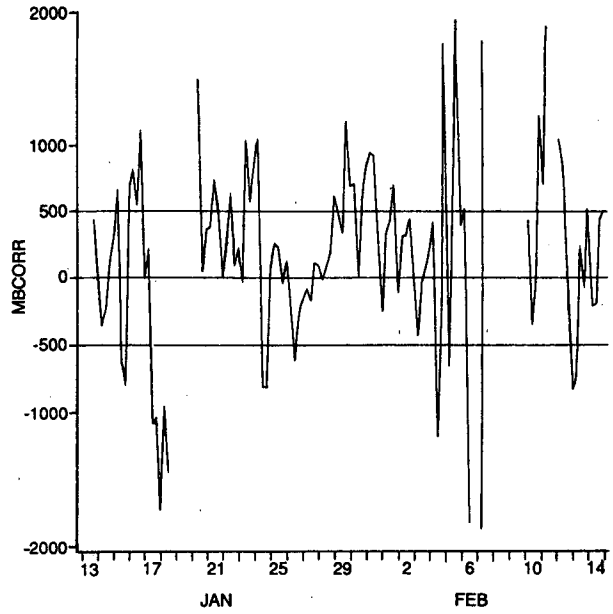

FIG. 9. Time series of mass-balance correction (mb day^{-1}) for the four station network Gove, Weipa, Thursday Island, and the PRC ship. Blanks correspond to times when the correction is off the graph; i.e., it exceeds 2000 mb day^{-1} in magnitude.

The time series of budget quantities for the complete array subject to the MBC threshold, showed many similarities to the time series of Frank (1979) for GATE. From the physical plausibility of the above results, it is believed the budget calculations are of sufficient quality to be useful in many follow-up studies on such topics as the specification of the vertical distribution of the heat and moisture source terms, the life cycles of individual weather systems, the changes in atmospheric structure leading up to tropical cyclogenesis, and diagnostic studies relevant to the problem of cumulus parameterization.

One of the major findings of the current study is that the diurnal variation of sensible warming (or observed rate of temperature change) throughout the depth of the troposphere has a magnitude comparable to the terms $[S_0, Q_R^*, L(\partial q/\partial t)^*, LE_0]$ of Eqs. (1) and (2). In particular, the sensible warming is of comparable magnitude to the sum $[\nabla \cdot sv^* - L\nabla \cdot qv^*]$ of the two flux divergence terms.

Both the magnitude of the diurnal variation of temperature and its independence of the presence or absence of convection have been previously documented by Foltz and Gray (1979) and by Frank (1980). It has

Unauthenticated | Downloaded 06/20/24 09:23 PM UTC

not, however, been realized that the term, $(\partial s/\partial t)^*$, is large enough to be important in diagnostic studies of the convective heat source and moisture sink, and by implication, in observational verifications of cumulus parameterization schemes.

REFERENCES

Albright, M. D., D. R. Mock, E. E. Recker and R. J. Reed, 1981: A diagnostic study of the diurnal rainfall variation in the GATE B-scale area. *J. Atmos. Sci.*, **38,** 1429–1445.

Anthes, R. A., 1974: The dynamics and energetics of mature tropical cyclones. *Rev. Geophys. Space Phys.*, **3,** 495–522.

——, 1977: A cumulus parameterization scheme utilizing a one-dimensional cloud model. *Mon. Wea. Rev.*, **105,** 270–286.

Betts, A. K., 1978: Convection in the tropics. *Meteorology over the Tropical Oceans*, Roy Meteor. Soc., 105–132.

Charney, J. G., and A. Eliassen, 1964: On the growth of the hurricane depression. *J. Atmos. Sci.*, **21,** 68–75.

Cox, S. K., and K. T. Griffith, 1979: Estimates of radiative divergence during Phase III of the GARP Atlantic Tropical Experiment. Part II: Analysis of Phase III results. *J. Atmos. Sci.*, **36,** 586–601.

Foltz, G. S., and W. M. Gray, 1979: Diurnal variation in the troposphere's energy balance. *J. Atmos. Sci.*, **36,** 1450–1466.

Frank, W. M., 1977: The structure and energetics of the tropical cyclone. Part II: Dynamics and energetics. *Mon. Wea. Rev.*, **105,** 1136–1150.

——, 1979: Individual time period analyses over the GATE ship array. *Mon. Wea. Rev.*, **107,** 1600–1616.

——, 1980: Modulations of the net tropospheric temperature during GATE. *J. Atmos. Sci.*, **37,** 1056–1064.

Gill, A. E., 1980: Some simple solutions for heat induced tropical circulation. *Quart. J. Roy. Meteor. Soc.*, **106,** 447–462.

Gray, W. M., 1973: Cumulus convection and larger scale circulations. Part I: Broadscale and mesoscale considerations. *Mon. Wea. Rev.*, **101,** 839–855.

Gunn, B. W., J. L. McBride, G. J. Holland, T. D. Keenan, N. E. Davidson and H. H. Hendon, 1989: The Australian summer monsoon circulation during AMEX Phase II. *Mon. Wea. Rev.*, **117,** 2554–2574.

Hack, J. J., and W. H. Schubert, 1986: Nonlinear response of atmospheric vortices to heating by organized cumulus convection. *J. Atmos. Sci.*, **43,** 1559–1573.

Krishnamurti, T. N., M. Kanamitsu, R. Godbole, C. B. Chang, F. Carr and J. H. Chow, 1976: Study of monsoon depression. II: dynamical structure. *J. Meteor. Soc. Japan.*, **54,** 208–226.

Kuo, H. L., 1974: Further studies of the parameterization of the influence of cumulus convection of large-scale flow. *J. Atmos. Sci.*, **31,** 1232–1240.

Lau, K. M., and L. Peng, 1987: Origin of low-frequency (intra-seasonal) oscillations in the tropical atmosphere. Part I: Basic theory. *J. Atmos. Sci.*, **44,** 950–972.

McBride, J. L., 1981: Observational analysis of tropical cyclone formation. Part III: Budget analysis. *J. Atmos. Sci.*, **38,** 1152–1166.

——, and G. J. Holland, 1989: The Australian monsoon experiment (AMEX): Early results. *Aust. Meteor. Mag.*, **37,** 23–35.

Newell, R. E., J. W. Kidson, D. G. Vincent and G. J. Boer, 1974: *The General Circulation of the Tropical Atmosphere and Interactions with Extratropical Latitudes.* Vol. 2. The MIT Press, 371 pp.

Ooyama, K. V., 1982: Conceptual evolution of the theory and modelling of the tropical cyclone. *J. Meteor. Soc. Japan.*, **60,** 369–380.

Puri, K., 1985: Sensitivity of low-latitude velocity potential field in a numerical weather prediction model to initial conditions, initialization and physical processes. *Mon. Wea. Rev.*, **113,** 449–466.

Silva Dias, P. L., W. H. Schubert and M. DeMaria, 1983: Large-scale response of the tropical atmosphere to transient convection. *J. Atmos. Sci.*, **40,** 2689–2707.

Song, J. L., and W. M. Frank, 1983: Relationships between deep convection and large-scale processes during GATE. *Mon. Wea. Rev.*, **111,** 2145–2160.

Syono, S., and M. Yamasaki, 1966: Stability of symmetrical motions driven by latent heat released by cumulus convection under the existence of surface friction. *J. Meteor. Soc. Japan.*, **44,** 353–375.

Yanai, M., S. Esbensen and J. H. Chu, 1973: Determination of bulk properties of tropical cloud clusters from large-scale heat and moisture budgets. *J. Atmos. Sci.*, **30,** 611–627.

Unauthenticated | Downloaded 06/20/24 09:23 PM UTC